Synthesis of Reconfigurable and Scalable Single-Inductor Multiport Converters with No Cross Regulation

Xiaolu Lucia Li, *Member, IEEE*, Chi K. Tse, *Fellow, IEEE*, and Dylan D.-C. Lu, *Senior Member, IEEE*

***Abstract*—This paper addresses the design of reconfigurable single-inductor multiport converters with bidirectional power flow, no cross regulation, and simple control. The design uses both voltage-source-mode cells and current-source-mode cells, thus allowing a full range of connectivity. The proposed single-inductor converters offer high modularity and scalability while offering bidirectional power flow and no cross regulation. The single-inductor structure reduces the overall size. The adoption of voltage-source-mode and current-source-mode cells leads to high modularity. High scalability is achieved due to arbitrary ports being allowed to the derived converters. Moreover, the topology inherently achieves no cross regulation among the output ports. The ports of the derived converters are reconfigurable, permitting transformation among single-input multi-output mode, multi-input multi-output mode, and multi-input single-output mode. Through transformation of operating modes, bidirectional power flow is achieved. Thus, regenerative loads can be integrated seamlessly. In terms of control, the absence of cross regulation permits the adoption of very simple control design, leading to high flexibility. Thus, the derived converters can integrate multiple and various kinds of terminating sources and loads simultaneously with simple control methods. A reconfigurable single-inductor four-port converter is presented for illustration. Finally, experimental results are presented to verify the analytical findings.**

***Index Terms*—Reconfigurable converter, single inductor, cross regulation, dc-dc converter, multiport converter.**

I. Introduction

MULTI-SOURCE multi-load structures become popular for combining diverse sources and loads simultaneously with the development of renewable energy sources and the explosive growth in electrical and electronic devices [1]–[6]. Particularly, the multiport dc-dc converter is attracting more attention. As a promising alternative of the conventional dc-dc system architecture with multiple converters, the multiport dc-dc converter has less components, fewer power conversion stages, and lower cost [7]–[10].

Nevertheless, some significant issues of multiport converters, including multiple-inductor structures, cross-regulation problem, and low integrating flexibility of regenerative loads, still need to be addressed. In much of the previous work, quite a few proposed converters have more than one inductor [11]–[15]. Multiple inductors will reduce the power density and increase the electromagnetic interference. With the increase of input/output ports, these disadvantages will be more obvious. Therefore, the single-inductor multiport converter is a more attractive solution. However, many single-inductor multiport converters cannot avoid the cross-regulation problem due to the common inductor [16]–[18]. Generally, the cross regulation among output ports will significantly affect the performance of a multiport converter and increase the corresponding control complexity [19]. To suppress the cross-regulation problem, various approaches based on control strategies and topological modifications have been adopted. These proposed control strategies, such as predictive digital current control, model predictive voltage control, and deadbeat control, are inevitably complicated [20]–[25]. To avoid the cross-regulation problem through topological modifications, current-source-mode converters are adopted [26]–[28]. Since there is no cross-regulation problem, the corresponding control scheme can be extremely simple. However, these proposed converters have less flexibility when they are used to integrate regenerative loads, such as batteries. This is because no bidirectional power flow paths exist in the proposed converters. Therefore, it is difficult to apply these converters to hybrid energy systems. To enable different combinations of power flow within the multiport converters, some reconfigurable multiport converters [29]–[31] and bidirectional multiport converters [32], [33] are proposed. However, due to the inherent converter structures, these converters are limited to three ports. Further extension of ports for these converters may require more magnetics or even entirely different structure. Hence, it significantly limits their potential for multiple-port applications.

In this paper, we attempt to present a systematic design pathway of reconfigurable single-inductor multiport converters with bidirectional power flow and no cross regulation. The proposed converters require very simple control and achieve high modularity and scalability. The ports of the proposed converters can be configured as input ports or output ports according to different application requirements. Therefore, the proposed converters can realize the transformation among

Manuscript received December 8, 2021; revised February 20, 2022. This work is supported by City University of Hong Kong Projects 7005463 and 9610515. *(Corresponding Author: Xiaolu Lucia Li)*

X. L. Li and C. K. Tse are with the Department of Electrical Engineering, City University of Hong Kong, Kowloon, Hong Kong. (Email: xiaoluli@cityu.edu.hk, cktse@ieee.org)

D. D-C. Lu is with the School of Electrical and Data Engineering, University of Technology Sydney, Broadway, NSW 2007, Australia. (Email: Dylan.Lu@uts.edu.au)

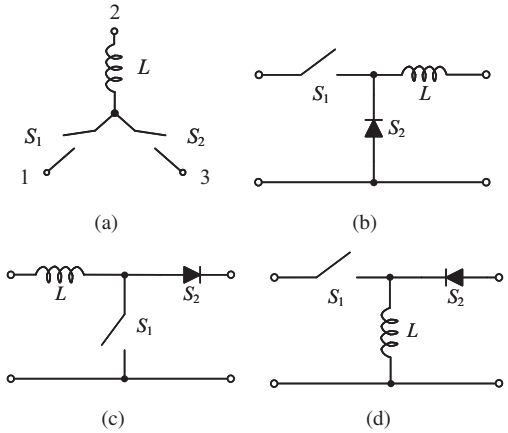

Fig. 1. Basic voltage-source-mode (a) cell; (b) buck converter; (c) boost converter; (d) buck-boost converter. Input terminals must be connected to voltage source.

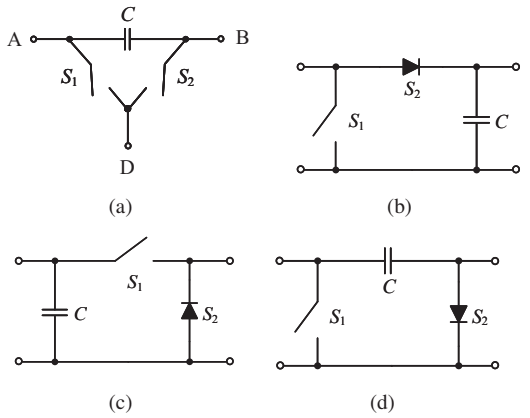

Fig. 2. Basic current-source-mode (a) cell; (b) buck converter; (c) boost converter; (d) buck-boost converter. Input terminals must be connected to current source.

single-input multi-output (SIMO), multi-input single-output (MISO) and multi-input multi-output (MIMO) converters. With reconfigurable ports, power can flow bidirectionally, and bidirectional loads can be integrated seamlessly. As inherited from the topology, there is no cross-regulation problem among output ports, thus drastically simplifying the control design. Moreover, the control principle remains the same regardless of the number of ports the converter has. Also, the single-inductor design is maintained for all configurations. The building blocks, i.e., voltage-source-mode cells and current-source-mode cells, enable high modularity. An arbitrary number of inputs/outputs is also achievable, leading to high scalability.

This paper is organized as follows. Section II presents a systemic derivation approach for the reconfigurable single-inductor multiport converters. The corresponding control principles are described in Section III. Section IV discusses detailed design considerations of the derived converters. An illustrative example is given in Section V to show how the derived converter works. Experimental results of the example are presented in Section VI to demonstrate the derivation of the proposed converters and the corresponding control design. Section VII presents some practical considerations for topology selection. Finally, Section VIII concludes the paper.

II. Topology Derivation

The synthesis procedure starts with the basic voltage-source-mode (VSM) cells and current-source-mode (CSM) cells. Different connection styles of the basic cells at the input side and the output side would lead to conventional MIMO converters. On this basis, reconfigurable paths will be constructed for the conventional MIMO converters to achieve the transformation between input cells and output cells.

A. Basic VSM and CSM Cells

The basic VSM cell includes one inductor and two switches, as shown in Fig. 1(a). The input of the VSM cell is a voltage source. Through connecting different pairs of terminals of the VSM cell to the input voltage source and the output load, we can obtain conventional dc-dc converters, i.e., buck converter, boost converter, and buck-boost converter. Applying the circuit duality principle to the basic VSM cell [28], [34], [35], we can obtain the basic CSM cell shown in Fig. 2(a), including one capacitor and two switches. Likewise, CSM dc-dc converters can be derived. The derived VSM converters and CSM converters are shown in Figs. 1 and 2, respectively.

In a VSM converter, the duty cycle directly controls the input-to-output voltage ratio, whereas in a CSM converter, the duty cycle directly controls the input-to-output current ratio. For a VSM converter, the relationship between input voltage and output voltage in the steady state is

$$V_{\rm o} = F(D)V_{\rm in},\ F(D) = \begin{cases} D & \text{VSM buck converter} \\ \frac{1}{1-D} & \text{VSM boost converter} \\ \frac{D}{1-D} & \text{VSM buck-boost converter} \end{cases} \tag{1}$$

where $V_{\rm in}$ is the input voltage, $V_{\rm o}$ is the output voltage, D is the steady-state duty cycle, and $F(.)$ is the function representing the input-to-output voltage transfer ratio. The relationship between input current and output current of a CSM converter, according to duality transformation, can be obtained by complementing the switch statuses, i.e., swapping open and closed switches, giving

$$I_{\rm o} = F'(D)I_{\rm in},\ F'(D) = \begin{cases} 1-D & \text{CSM buck converter} \\ \frac{1}{D} & \text{CSM boost converter} \\ \frac{1-D}{D} & \text{CSM buck-boost converter} \end{cases} \tag{2}$$

where $I_{\rm in}$ is the input current, $I_{\rm o}$ is the output current, D is the steady-state duty cycle, and $F'(.)$ is the function representing the input-to-output current transfer ratio.

B. Connection Rules of VSM and CSM Cells

Since VSM cells and CSM cells are the basic building blocks of the proposed converters, the connections of selected VSM cells and CSM cells should ensure no cross regulation while keeping the single-inductor structure.

According to the above expressions, the output voltage of a VSM converter only relates to the corresponding input voltage and duty cycle. However, when a VSM converter is employed

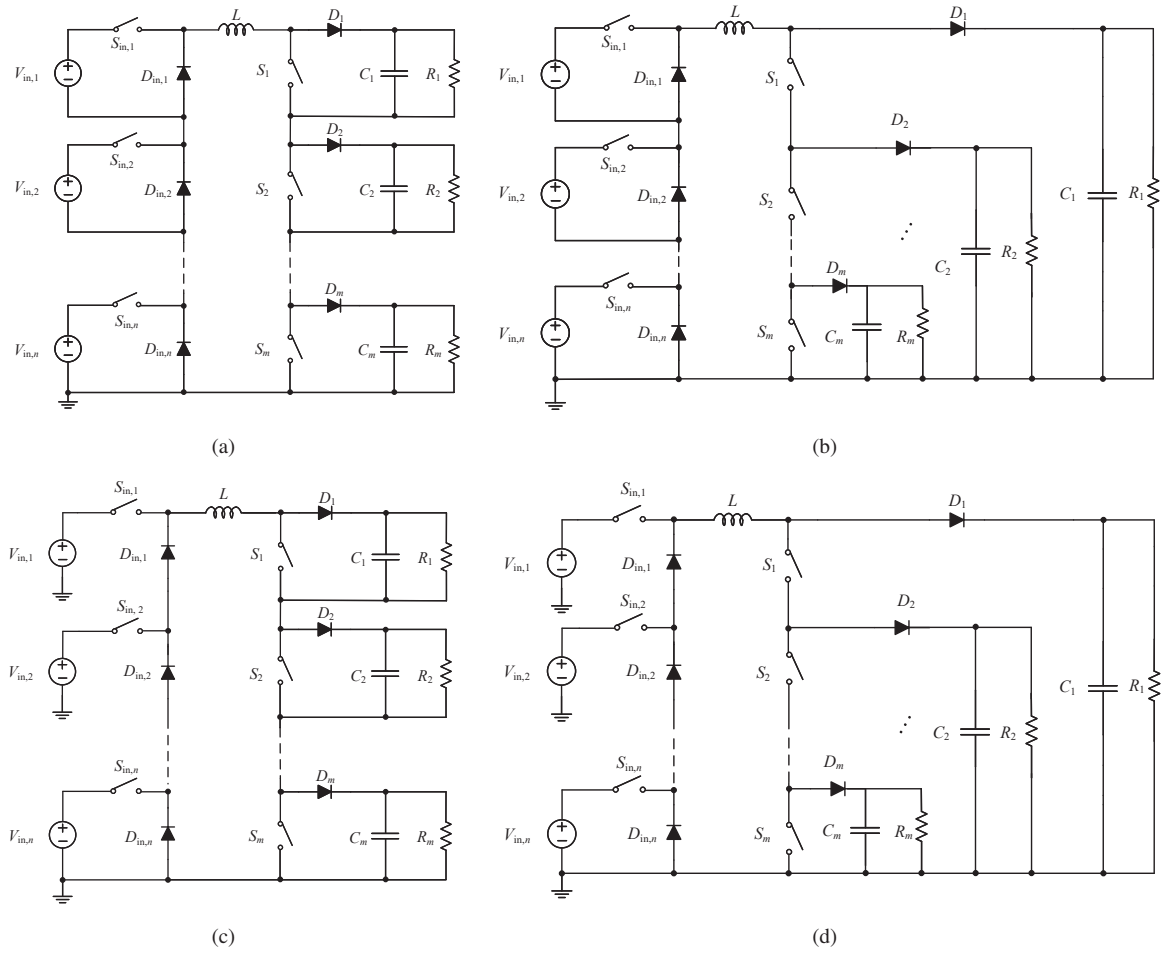

Fig. 3. Conventional MIMO converters. "S" means series connection, and "P" means quasi-parallel connection. (a) SS connection (no common ground); (b) SP connection (output common ground); (c) PS connection (input common ground); (d) PP connection (all ports having common ground).

to deliver regulated current to a load, current-programming control (commonly called current-mode control) is necessary. This is because the output current of a VSM converter depends not only on the input voltage and duty cycle but also the load resistance. Likewise, the output current of a CSM converter only relates to the corresponding input current and duty cycle, while the output voltage of a CSM converter is dependent on the input current, duty cycle and load resistance. The input voltage of a CSM converter is then determined.

On this basis, it should be clear that VSM cells interconnecting at the input side are independent of each other as long as they share the same input voltage, e.g., in parallel-connected VSM cells. Likewise, CSM cells interconnecting at the input side are also independent of each other if they share the same input current, e.g., in series-connected CSM cells [36]. Thus, in our derivation of reconfigurable multiport converters, CSM cells with the same input current are the natural choice to realize the single-inductor design which inherently avoids cross regulation. Moreover, the use of VSM cells and CSM cells permits high modularity.

C. Derivation of Single-Inductor MIMO Converters

Conventional MIMO converters can be derived from connecting VSM and CSM cells in a variety of ways. As input sources are generally voltage sources, basic VSM cells are used as input cells of MIMO converters. Besides, we specify that the MIMO converter contains only one inductor, i.e., all VSM cells should share one inductor. Therefore, the inductor should be placed at the end of the VSM cell. Under this condition, the VSM buck cell is the only choice. For the output side, the CSM buck cell should be used as it has no inductor and its capacitor can be used to ensure a constant input voltage when the output port is reconfigured as an input port.

Four single-inductor MIMO converters can be generated by connecting the input VSM buck cells and output CSM buck cells as shown in Fig. 3. For the converter in Fig. 3(a), both input-side cells and output-side cells are connected in series. Thus, the input sources and output loads have no common ground. For the converter in Fig. 3(b), the switches at the inputs of the output cells (i.e., S_1, S_2, etc.) are connected in series while the other components of the output cells are connected in parallel. We refer to this connection style as *quasi-parallel* connection style. Series connection of the switches of CSM buck cells ensures that the input current of each cell is equal by applying very simple control. On the other hand, the parallel connection of the rest of the components of the CSM buck cells provides a common ground for the output ports, as shown in Fig. 3(b). For the quasi-parallel connection

of the input cells, as given in Fig. 3(c), the diodes of the input cells are connected in series while the corresponding sources and switches are connected in parallel. As a result, the input ports of the converter in Fig. 3(c) can share a common ground while the output ports are floating. Finally, all ports of the converter shown in Fig.3(d) have a common ground.

D. Derivation of Reconfigurable Multiport Converters

To obtain reconfigurable multiport converters, reconfigurable paths need to be constructed in the conventional MIMO converters. If one port is assigned either as an input port or an output port, this port should have paths for supplying and consuming power. Here, we take the derivation of a reconfigurable single-inductor multiport converter with series-connected input ports and output ports as an example for illustration.

One input port and one output port of a conventional MIMO converter with series-connected input ports and output ports are shown in Fig. 4(a). To clearly show how the input port and the output port can be redesigned as one reconfigurable port, we rearrange the positions of the input and output ports, as shown in Fig. 4(b). Suppose we want a reconfigurable port that can be assigned as either an input port or an output port. This reconfigurable port must be connected to both the input and output sides. Initially, we use one port (i.e., $F_{\rm in}/F_{\rm o}$) to replace the input port connecting $V_{\rm in}$ and the output port connecting R simultaneously, as shown in Fig. 4(c). Here, we note that the input port and the output port have different power flow directions. Path 1, marked in red, is the theoretical power flow path of the input port. Paths 2 and 3, marked in blue, form the theoretical power flow path of the output port. When we replace the input and output ports with one reconfigurable port, we need to maintain the previous power flow direction. Therefore, switches are added to the corresponding paths to ensure the initial power flow direction. Also, the diode of the previous output port is replaced by a switch. The resulting reconfigurable structure is shown in Fig. 4(d). Other reconfigurable ports can be obtained in a likewise manner. The derivation steps of the other three reconfigurable converters are summarized in Figs. 5, 6, and 7.

The converters with reconfigurable paths are shown in Fig. 8. For the converters with all ports having a common ground, only the diodes of the output cells are replaced by switches to cut off the power flow path of the output side when the output cells are reconfigured as input cells. For the converters without a common ground of all ports, two more switches are added for one reconfigurable port in order to guarantee the expected power flow direction.

Based on the above discussions, the design steps are summarized as follows:

1) *Determination of input-side VSM cells and output-side CSM cells:* CSM cells are adopted as output cells to avoid cross regulation. VSM buck cells and CSM buck cells are adopted to give single-inductor converters.
2) *Selection of connection styles of input and output cells:* Series connection is used in situations without common-ground requirement. Quasi-parallel connection provides a common ground to all interconnected cells.

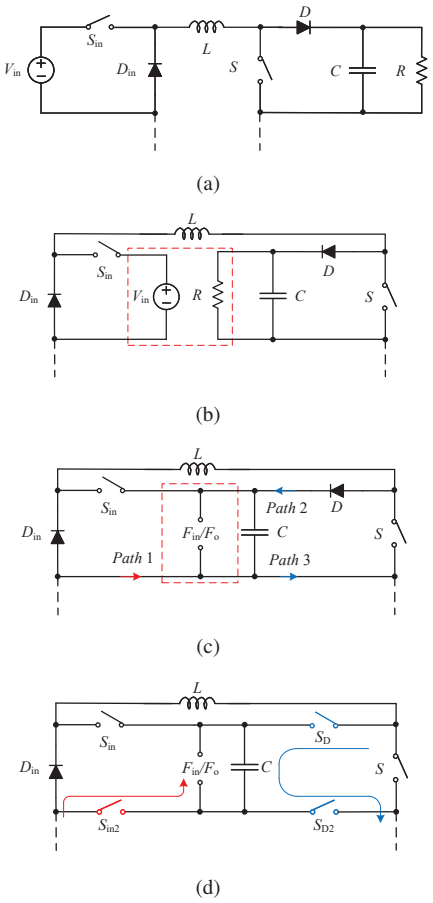

Fig. 4. Reconfigurable multiport converter with SS connection. (a)–(d) Step-by-step derivation. Paths marked in blue indicate the power flow direction of the output port, and paths marked in red indicate the power flow direction of the input port.

3) *Derivation of a conventional MIMO converter:* A conventional MIMO converter can be obtained through various connection styles of input cells and output cells.
4) *Construction of reconfigurable paths:* To obtain a reconfigurable port, one port is used to replace one input port and one output port of the conventional MIMO converter at the same time. The reconfigurable port is connected to the input terminal of one input cell and the output terminal of one output cell simultaneously. Configuration switches are added to vary the power flow direction when necessary.

III. Control

The control design of the proposed multiport converters will be discussed for the input-side and output-side converters.

A. Control of Input Converters

For the proposed multiport converters, CSM cells are selected as output cells. CSM cells require a regulated input current. Therefore, a constant inductor current is essential. This means the key control principle for the input side is to provide a regulated current for the output side.

Three possible configurations for providing a constant current are shown in Fig. 9. The input-side converters are expected

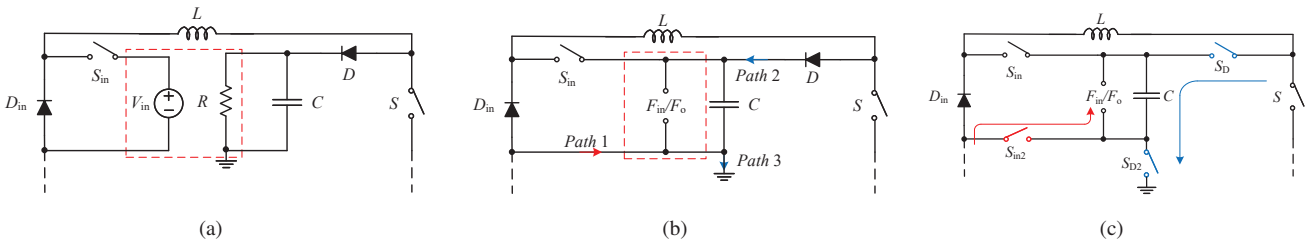

Fig. 5. Reconfigurable multiport converter with SP connection. (a)–(c) Step-by-step derivation.

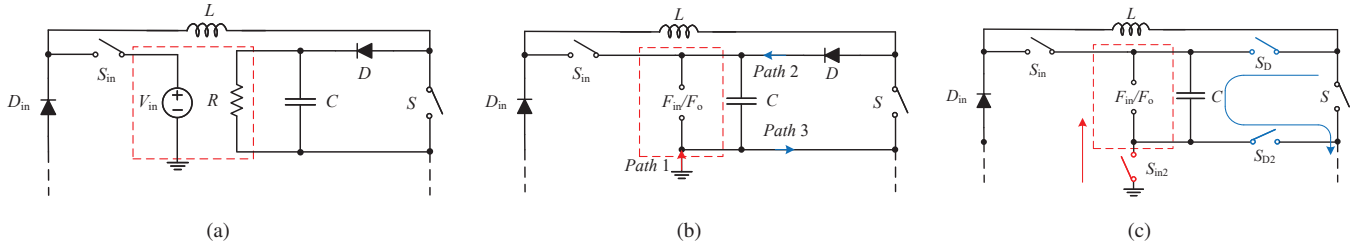

Fig. 6. Reconfigurable multiport converter with PS connection. (a)–(c) Step-by-step derivation.

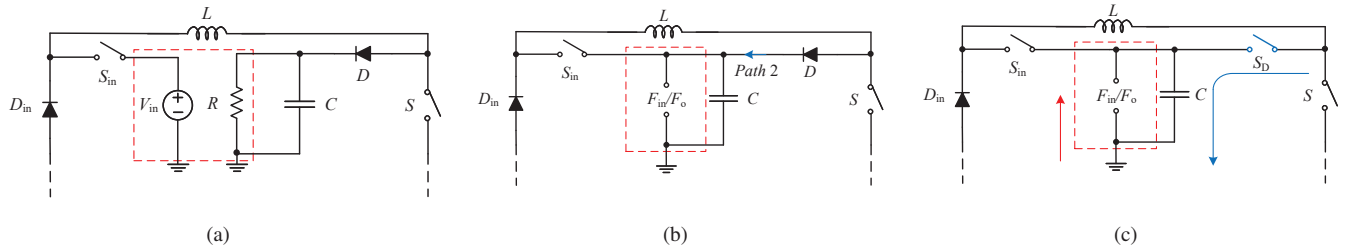

Fig. 7. Reconfigurable multiport converter with PP connection. (a)–(c) Step-by-step derivation.

to behave as controlled sources to their downstream (output-side) converters. The output-side converters can be modeled as an equivalent load $R_{\rm eq}$. For the series-connected input-side converters, there are two control methods to provide a constant current. One method is to apply closed-loop control to all series-connected input-side converters. In this situation, all input-side converters can be viewed as one controlled current source. The equivalent circuit is shown in Fig. 9(a). Inductor current $I_{\rm mid}$ is equal to the reference current I. Another method is to apply closed-loop control to some of the input-side converters, leaving the remaining input-side converters to be controlled via direct duty-cycle control. Under this condition, the closed-loop controlled input-side converters can be viewed as one controlled current source and the direct duty-cycle controlled input-side converters effectively controlled voltage sources. Since these controlled sources are connected in series as shown in Fig. 9(b), $I_{\rm mid}$ is still equal to I.

For the quasi-parallel-connected input-side converters, two possibilities exist to provide a constant current. With the constant current control, the input-side converters are equivalent to controlled current sources, as shown in Fig. 9(c). When the controlled current sources provide power at the same time, $I_{\rm mid} = I_1 + I_2 + \cdots + I_n$. However, more inductors will be needed in this case. Therefore, time multiplexing control should be applied to the input-side converters to ensure $I_{\rm mid} = I_1 = I_2 = \cdots = I_n$. This control requires that only one source provides power at a time.

B. Control of Output Converters

Cross regulation is the key issue for single-inductor multiport converters when there are multiple output ports. Cross regulation will require a complicated control scheme. Therefore, our design aims to inherently avoid cross regulation among the output-side converters.

It should be obvious that interconnected VSM converters with the same input voltage are independent of each other. Likewise, interconnected CSM converters with the same input current are also independent of each other. Thus, there is no cross regulation issue among the output-side converters of the derived converters if all output-side converters are fed by the same input current. For the series-connected CSM cells, they are naturally decoupled since these cells have the same input current supplied by the inductor. Therefore, direct duty-cycle control can satisfy the basic output requirement. For the quasi-parallel-connected CSM cells, only the switch of the working cell is open, while the other switches connected in series are closed, thus ensuring that the input current of each CSM (output-side) cell is identical. Thus, time multiplexing control is necessary for the quasi-parallel-connected output-side converters.

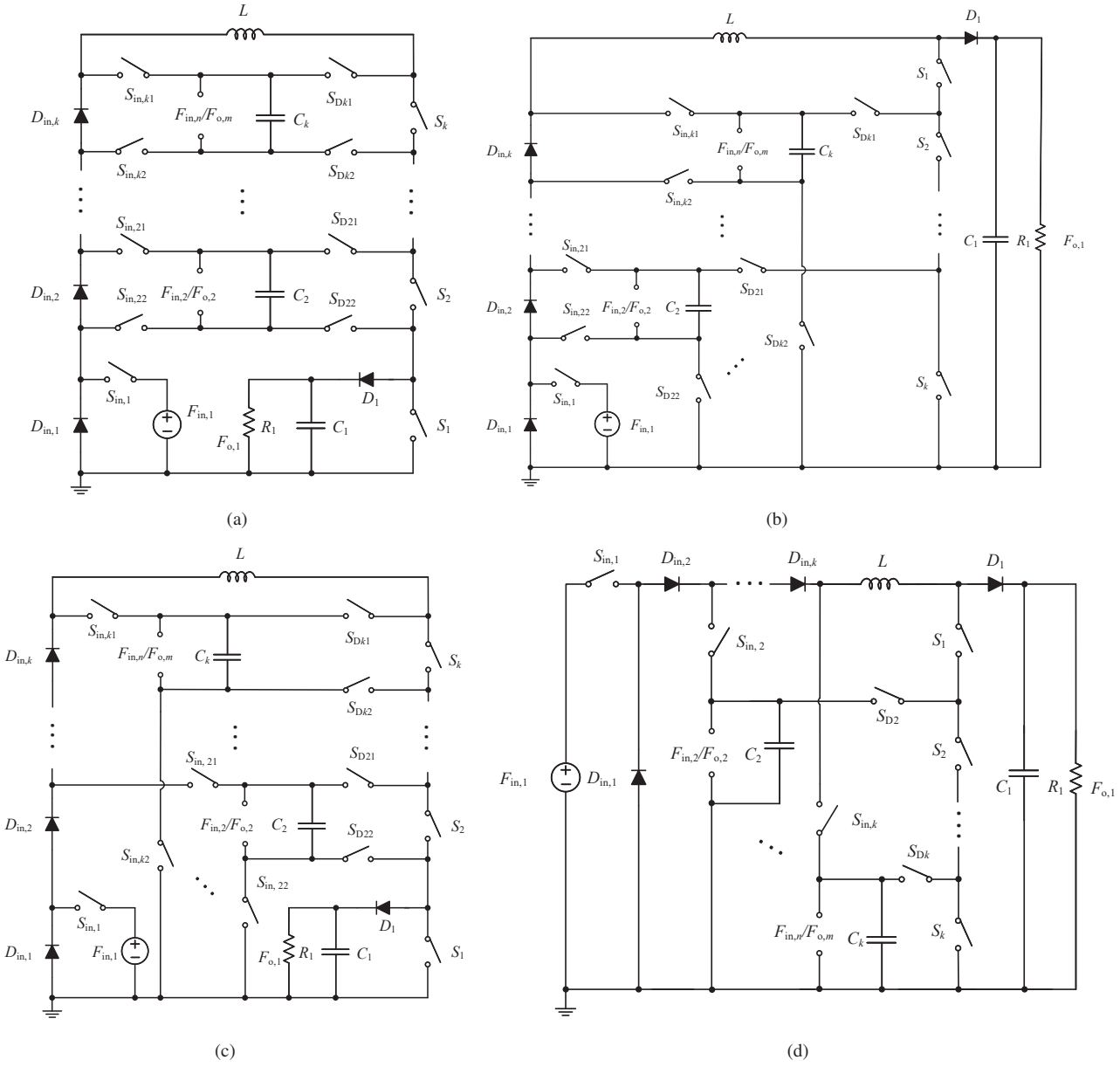

Fig. 8. Reconfigurable single-inductor MIMO converters. (a) SS connection; (b) SP connection; (c) PS connection; (d) PP connection. $F_{\text{in}}/F_{\text{o}}$ indicates reconfigurable input or output port.

C. Guideline of Control Selection

From the above analysis, the control design flow chart for the derived converters is obtained, as shown in Fig. 10. Suitable control methods can be determined based on the presented flow chart along with connection styles of the input side and output side.

Constant current control of the input side is always necessary to ensure a regulated inductor current. Time multiplexing control of the input side with quasi-parallel connection should ensure that there is only one source providing power at a time. In other words, among $S_{\text{in},1}$, $S_{\text{in},21}$ (or $S_{\text{in},2}$), $\cdots$, $S_{\text{in},k1}$ (or $S_{\text{in},k}$), there is only one switch being closed at a time. Time multiplexing control of the output side with quasi-parallel connection should ensure that there is only one output cell working at a time. Thus, among S_1, S_2, $\cdots$, S_k, only one of them is open at a time. Since cross regulation is inherently avoided, no extra control is needed.

Remark: In terms of topology, the multiport converter shown in Fig. 8(d) is a preferred choice. This topology uses fewest switches and simply involve replacing the diodes of the output-side converters by switches. The alternative switches stop the power from flowing into the converters when being configured as input-side converters. Besides, all ports have a common ground. In terms of control, moreover, the multiport converter shown in Fig: 8(a) is the preferred choice because no time multiplexing control is needed. As there is no cross regulation among the output-side converters, the corresponding control design is simple and straightforward.

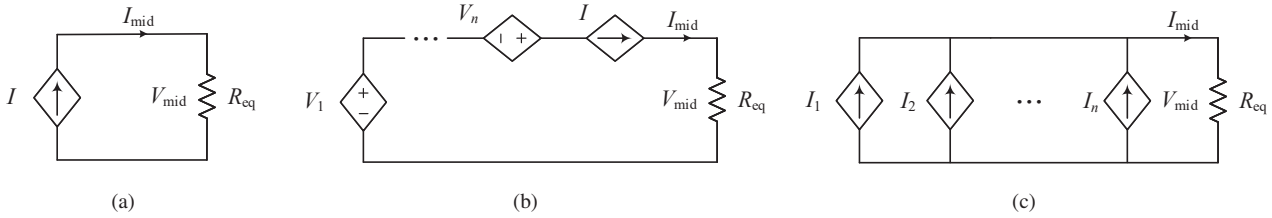

Fig. 9. Equivalent circuits for controlling the output current of the input-side converters. Here, I, I_1, $\cdots$, I_n are regulated through controlling the input-side converters, V_1, $\cdots$, V_n are the output voltage of the input-side converters without constant current control, and I_{mid} is the inductor current. Output-side converters are equivalent to load R_{eq}. (a) Control scheme of series-connected input-side converters; (b) alternative control scheme of series-connected input-side converters; (c) control scheme of quasi-parallel-connected input-side converters.

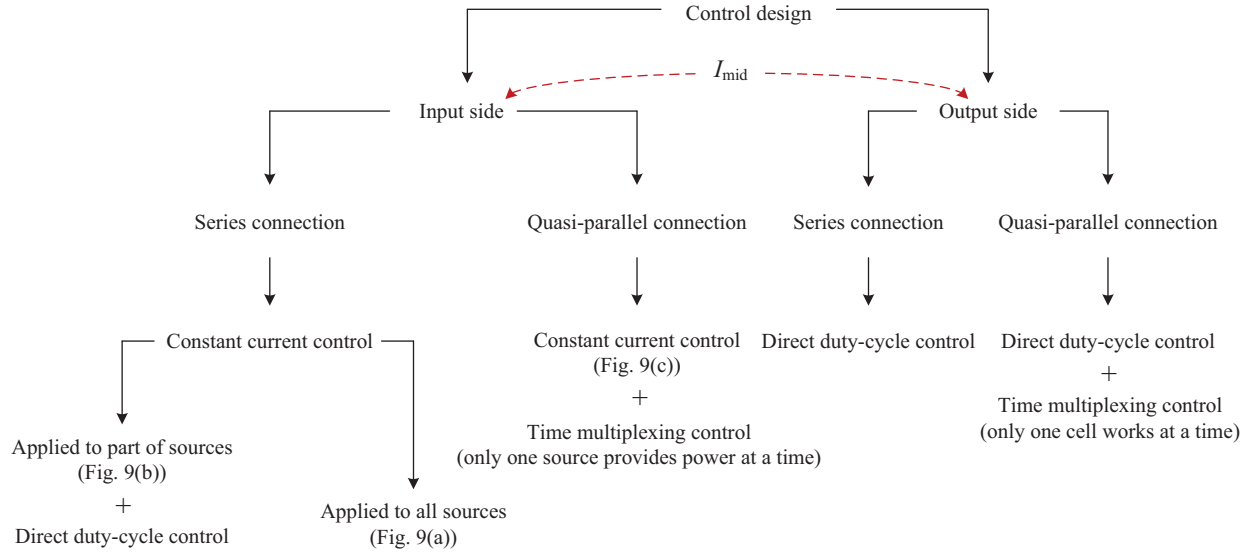

Fig. 10. Control flow chart for the derived converters.

IV. Design Considerations

A. Selection of Inductor Current

As the key parameter of the whole control scheme, the inductor current reference is significant. To ensure the proper operation of the derived converters, the input power and output power of each converter should satisfy the relationship $P_{\text{in,max}} > P_{\text{o}}$, where $P_{\text{in,max}}$ is the maximum input power and P_{o} is the output power.

1) Series Connection of Input Cells: Assume there are n input ports and m output ports, the maximum power provided by the input sources for series-connected input cells can be expressed as

$$P_{\text{in,max}} = (V_{\text{in},1} + V_{\text{in},2} + \cdots + V_{\text{in},n}) I_{\text{mid}}. \tag{3}$$

The output cells are CSM buck converters with constant inductor current. Therefore, there is a direct relationship between the input current and the output current. Taking the first CSM cell as an example, the output current I_{o1} can be calculated using

$$I_{\text{o1}} = (1 - D_{\text{S1}}) I_{\text{mid}} \tag{4}$$

where D_{S1} is the duty cycle of S_1.

For m output ports, the output power can be expressed as follows:

$$P_{\text{o}} = P_{\text{o},1} + P_{\text{o},2} + \cdots + P_{\text{o},m}. \tag{5}$$

Then, the output power can be calculated using

$$P_{\text{o}} = (1 - D_{\text{S1}})^2 {I_{\text{mid}}}^2 R_1 + \cdots + (1 - D_{\text{S}m})^2 {I_{\text{mid}}}^2 R_m \tag{6}$$

where R_1, $\cdots$, R_m are equivalent output resistances of the corresponding output ports, D_{S2}, $\cdots$, $D_{\text{S}m}$ are duty cycles of S_2, $\cdots$, S_m, respectively.

Based on the above relationship, we obtain the selection principle of the inductor current, i.e.,

$$I_{\text{mid}} < \frac{V_{\text{in},1} + \cdots + V_{\text{in},n}}{(1 - D_{\text{S1}})^2 R_1 + \cdots + (1 - D_{\text{S}m})^2 R_m}. \tag{7}$$

2) Quasi-Parallel Connection of Input Cells: For the quasi-parallel-connected input cells, there is only one input source proving power at a time. Thus, the maximum input power can be expressed as

$$P_{\text{in,max}} = \max\{V_{\text{in},1}, \cdots, V_{\text{in},n}\} I_{\text{mid}}. \tag{8}$$

Thus, we get the selection principle of the inductor current for converters with quasi-parallel connection as

$$I_{\text{mid}} < \frac{\max\{V_{\text{in},1}, \cdots, V_{\text{in},n}\}}{(1 - D_{\text{S1}})^2 R_1 + \cdots + (1 - D_{\text{S}m})^2 R_m}. \tag{9}$$

TABLE I
VOLTAGE STRESS AND CURRENT STRESS OF SWITCHES AND DIODES

	Voltage stress	Current stress
$S_{\mathrm{in},k}$, $S_{\mathrm{in},k1}$, $S_{\mathrm{in},k2}$, $D_{\mathrm{in},k}$	$V_{\mathrm{in},k}$	I_{mid}
$S_{\mathrm{D}k}$, $S_{\mathrm{D}k1}$, $S_{\mathrm{D}k2}$, S_k, D_1	V_{ok}	I_{mid}

B. Inductor Design

To obtain a continuous input current for the output cells, the inductor design is important. Since the frequencies of input-side switches and output-side switches can be set independently, the inductor current can take various forms. Here, we consider the worst operating situation for reference. The design can be optimized according to specific frequency settings.

1) Series Connection of Output Cells: For the converter with series-connected output cells, the worst working condition is that there is only one source providing power to the output cells with all the input switches of the output cells (i.e., S_1, S_2, $\cdots$, S_m) being open. Under this condition, the input side of the proposed converter can be viewed as a buck converter with output voltage V_{S}. The output voltage V_{S} can be calculated according to $V_{\mathrm{S}} = V_{\mathrm{o}1} + V_{\mathrm{o}2} + \cdots + V_{om}$, where $V_{\mathrm{o}1}$, $V_{\mathrm{o}2}$, $\cdots$, V_{om} are the output voltages of the output cells.

Thus, the design of the inductor should satisfy the following inequality:

$$L \geq \frac{V_{\mathrm{o}1} + V_{\mathrm{o}2} + \cdots + V_{om}}{2 I_{\mathrm{mid}} f_{\mathrm{in}}} (1 - D_{\mathrm{in}}). \tag{10}$$

To ensure a continuous inductor current under the worst operating conditions, we should calculate $\frac{1-D_{\mathrm{in}}}{f_{\mathrm{in}}}$ according to

$$\frac{1 - D_{\mathrm{in}}}{f_{\mathrm{in}}} = \max\{\frac{1 - D_{\mathrm{in},1}}{f_{\mathrm{in},1}}, \frac{1 - D_{\mathrm{in},2}}{f_{\mathrm{in},2}}, \cdots, \frac{1 - D_{\mathrm{in},n}}{f_{\mathrm{in},n}}\} \tag{11}$$

where $D_{\mathrm{in},1}$, $D_{\mathrm{in},2}$, $\cdots$, $D_{\mathrm{in},n}$ are duty cycles of $S_{\mathrm{in},1}$, $S_{\mathrm{in},2}$, $\cdots$, $S_{\mathrm{in},n}$, respectively, and $f_{\mathrm{in},1}$, $f_{\mathrm{in},2}$, $\cdots$, $f_{\mathrm{in},n}$ are switching frequencies of $S_{\mathrm{in},1}$, $S_{\mathrm{in},2}$, $\cdots$, $S_{\mathrm{in},n}$, respectively.

2) Quasi-Parallel Connection of Output Cells: For the converter with quasi-parallel-connected output cells, the worst working condition is that there is only one source providing power to the output cell with maximum output voltage as there is only one output cell working at a time. In this case, the inductor value should satisfy the following inequality:

$$L \geq \frac{\max\{V_{\mathrm{o}1}, V_{\mathrm{o}2}, \cdots, V_{om}\}}{2 I_{\mathrm{mid}} f_{\mathrm{in}}} (1 - D_{\mathrm{in}}). \tag{12}$$

C. Voltage and Current Stresses

To facilitate selection of power devices, the voltage and current stresses of the semiconductor devices are presented in Table I.

V. ILLUSTRATION OF OPERATION

To verify the theoretical analysis of the proposed reconfigurable multiport converters, we take a four-port converter with PP connection as an illustration. There are three working modes of the converter, as shown in Fig. 8(d), i.e., SIMO mode, MIMO mode, and MISO mode.

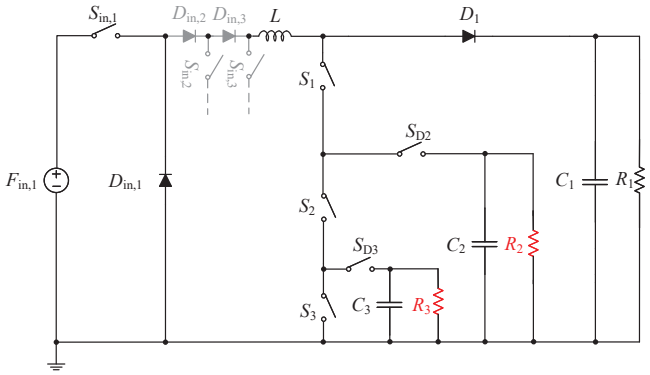

Fig. 11. Configured SIMO converter. To show different modes clearly, inactive switches and diodes are marked grey. The resistive loads marked red can be replaced by regenerative loads.

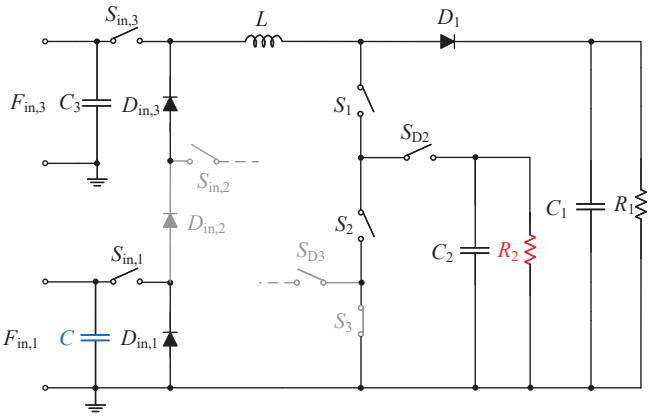

Fig. 12. Configured MIMO converter.

To achieve a single-input three-output working mode shown in Fig. 11, switches $S_{\mathrm{in},2}$ and $S_{\mathrm{in},3}$ need to be open. If we want a dual-input dual-output converter, we can configure one of $F_{\mathrm{in},2}$/$F_{\mathrm{o},2}$ and $F_{\mathrm{in},3}$/$F_{\mathrm{o},3}$ as the input port and the other as the output port, as shown in Fig. 12. Moreover, a three-input single-output converter can be achieved when switches $S_{\mathrm{D}2}$, $S_{\mathrm{D}3}$ are open and switches S_2, S_3 are closed, as shown in Fig. 13. The capacitors marked in blue in Figs. 12 and 13 are added to ensure a constant voltage of $F_{\mathrm{in},1}$. The operating modes and the corresponding switch states are listed in Table II.

The control scheme for the input side and the output side can be derived following the control design flow chart shown in Fig. 10. Constant current control and time multiplexing control are necessary for the input side. Direct duty-cycle control and time multiplexing control are adopted for the output side. Time multiplexing control can be achieved with either analog or digital control schemes. For the given example, the drive signals of $S_{\mathrm{in},1}$, $S_{\mathrm{in},2}$, $S_{\mathrm{in},3}$, S_1, S_2 and S_3 after the time multiplexing scheme should satisfy the relationship shown in Table III regardless of the original drive signals. This is to ensure that only one source provides power at a time, and that the three series-connected switches S_1, S_2, and S_3 do not open simultaneously to avoid cross regulation among the output-side converters. When the number of input-side and output-side

TABLE II
OPERATING MODES AND SWITCH OPERATION LOOKUP TABLE

Modes	Power flow paths	$S_{\mathrm{in},1}$ and S_1	$S_{\mathrm{in},2}$	$S_{\mathrm{in},3}$	S_2 ($\overline{S_{\mathrm{D2}}}$)	S_3 ($\overline{S_{\mathrm{D3}}}$)
Mode 1 (SIMO)	$F_{\mathrm{in},1}$ to $F_{\mathrm{o},1}$, $F_{\mathrm{o},2}$, and $F_{\mathrm{o},3}$	Switching	Off	Off	Switching	Switching
Mode 2 (MIMO)	$F_{\mathrm{in},1}$ and $F_{\mathrm{in},3}$ to $F_{\mathrm{o},1}$ and $F_{\mathrm{o},2}$	Switching	Off	Switching	Switching	On
Mode 3 (MISO)	$F_{\mathrm{in},1}$, $F_{\mathrm{in},3}$, and $F_{\mathrm{in},3}$ to $F_{\mathrm{o},1}$	Switching	Switching	Switching	On	On

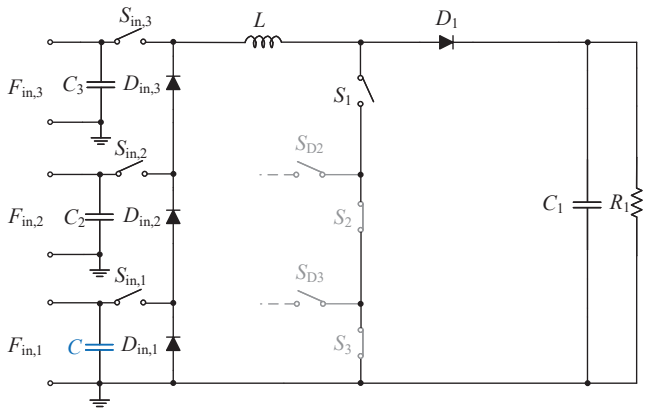

Fig. 13. Configured MISO converter.

TABLE III
TRUTH TABLE OF SIGNALS AT INPUT AND OUTPUT SIDES

Input Side			Output Side		
$Q_{\mathrm{in}1}$	$Q_{\mathrm{in}2}$	$Q_{\mathrm{in}3}$	$Q_{\mathrm{S}1}$	$Q_{\mathrm{S}2}$	$Q_{\mathrm{S}3}$
0	0	0	1	1	1
1	0	0	1	1	0
0	1	0	0	1	1
0	0	1	1	0	1

converters is less than the number of driving signals, only the corresponding driving signal needs to be removed.

VI. EXPERIMENTAL RESULTS

A laboratory prototype has been constructed to demonstrate the performance of the proposed single-inductor multiport converter using PP connection. The values of components and parameters are shown in Table IV.

A. SIMO Application

When the converter is configured as a SIMO converter, the driving signal of the input cell is shown in Fig. 14. Input voltage $F_{\mathrm{in},1}$ is 24 V. Inductor current I_{mid} is controlled to be 1.5 A. The driving signals of S_1, S_2 and S_3 are shown in Fig. 15. When one switch is off, the other two switches are on in order to ensure that the input current of the working output-side converter aligns with the inductor current. The working waveforms of each output-side converters are shown in Fig. 16. The output voltage and output current of the first output-side converter are 24 V and 300 mA, respectively. For the second output-side converter, the output voltage and current are 6 V and 750 mA, respectively. For the third output-side converter, the output voltage and current are 6 V and 400 mA, respectively.

TABLE IV
VALUES OF COMPONENTS IN EXPERIMENTAL CIRCUIT

Design parameter	Value
Input voltage $F_{\mathrm{in},1}$	24 V
Battery $F_{\mathrm{in},2}$	6 V
Battery $F_{\mathrm{in},3}$	6 V
Rated inductor current I_{mid}	1.5 A
Inductor L	1000 μH
Capacitor C_1	100 μF
Capacitor C_2	100 μF
Capacitor C_3	100 μF
Operating frequency $f_{\mathrm{in},1}$	55 kHz
Operating frequency $f_{\mathrm{in},2}$	80 kHz
Operating frequency $f_{\mathrm{in},3}$	100 kHz
Operating frequency f_{s}	55 kHz
Output current $i_{\mathrm{o}1}$	0.3 A
Output current $i_{\mathrm{o}2}$	0.75 A
Output current $i_{\mathrm{o}3}$	0.4 A
Load R_1	80 Ω / 120 Ω

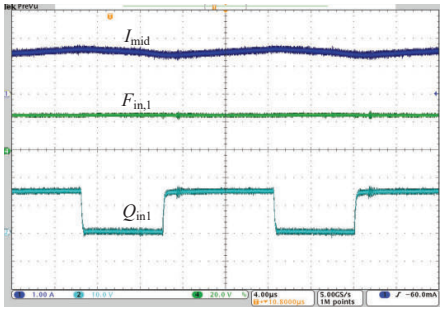

Fig. 14. SIMO working waveforms of the input-side converter and inductor current.

B. MIMO Application

When the converter is configured as an MIMO converter, the working waveforms of the input-side converters are shown in Fig. 17. Input voltage $F_{\mathrm{in},1}$ is 24 V and $F_{\mathrm{in},3}$ is 6 V. With the constant current control of input-side converters, I_{mid} is kept at 1.5 A.

The working waveforms of output-side converters are shown in Fig. 17(c). The output voltage and current of the first output-side converter are 24 V and 300 mA, respectively. For the second output-side converters, the output voltage and current are 6 V and 750 mA, respectively. The transient waveforms are shown in Fig. 18, when the load of the first output port

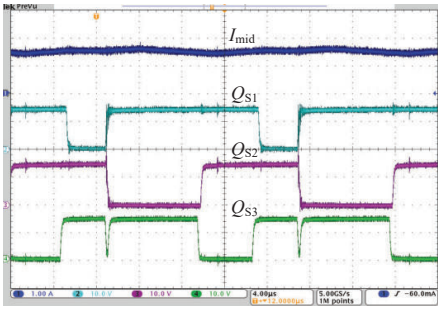

Fig. 15. Driving signals of S_1, S_2 and S_3 in SIMO configuration.

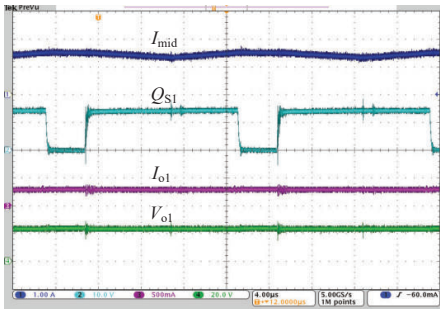

(a)

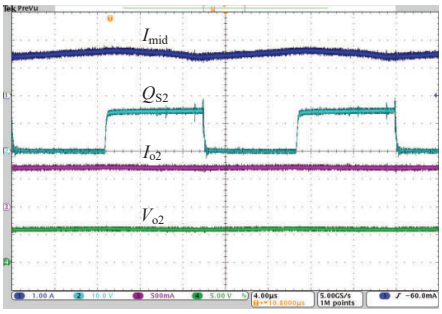

(b)

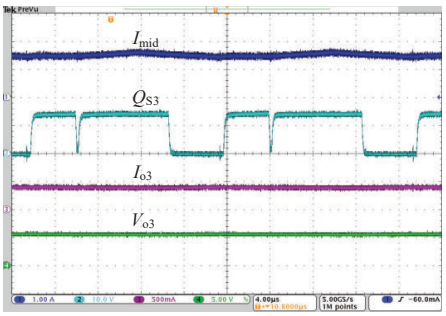

(c)

Fig. 16. SIMO working waveforms of (a) first output-side converter; (b) second output-side converter; (c) third output-side converter.

changes from 80 Ω to 120 Ω. The output current of the first output I_{o1} is still 300 mA, while the output voltage increases to 36 V because of the step change of R_1. Meanwhile, the second output port is unaffected. Based on the experimental results, we verify that the two output ports are independent of each other (i.e., no cross regulation) without using any extra control. Besides, it is obvious that the proposed converter can step up or down the input voltage.

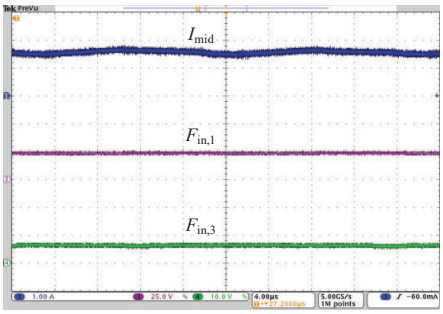

(a)

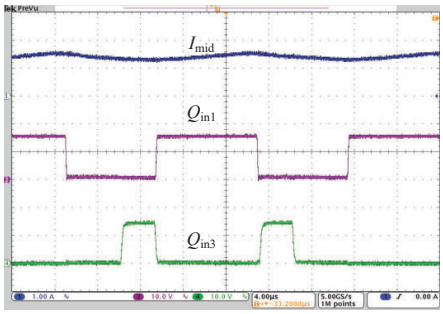

(b)

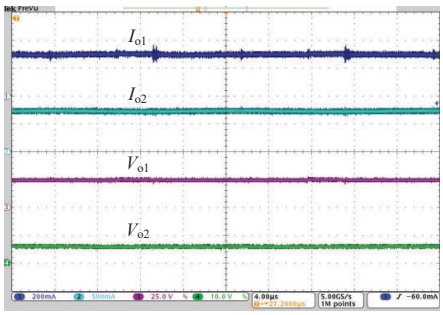

(c)

Fig. 17. MIMO working waveforms. (a) Input voltage and inductor current input-side converters; (b) driving signals of $S_{in,1}$ and $S_{in,3}$ of input-side converters; (c) output currents and voltages of output-side converters.

C. MISO Application

When the converter is configured as an MISO converter, the working waveforms of the input-side converters are shown in Fig. 19. Input voltage $F_{in,1}$ is 24 V and $F_{in,2}$ and $F_{in,3}$ are both 6 V. Inductor current I_{mid} is 1.5 A. Through the time multiplexing control, there is only one source providing power at a time. The working waveforms of the output-side converter are shown in Fig. 19(c). The output voltage and current are 24 V and 300 mA, respectively.

D. Bidirectional Power Flow of Reconfigurable Ports

For each of the operating modes described above, power flows into a reconfigurable port from the source when the reconfigurable port is configured as an input port, and power also flows out of the reconfigurable port to the load when the reconfigurable port is configured as an output port. Thus, bidirectional power flow is realized through assigning the reconfigurable ports as input ports and output ports at different times. The exact power flow directions of the reconfigurable

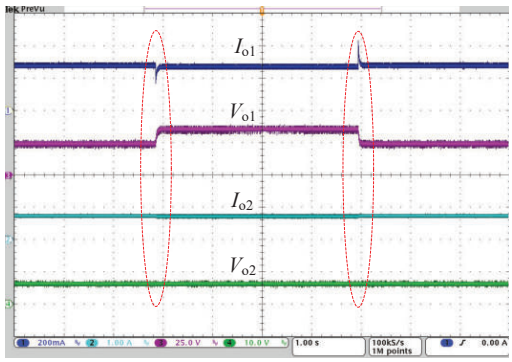

Fig. 18. MIMO transient waveforms of output-side converters when the load of the first output changes from 80 Ω to 120 Ω.

ports are summarized in Table II. To show the role transition of a reconfigurable port clearly, we present the corresponding waveforms of ports $F_{\mathrm{in},2}/F_{\mathrm{o},2}$ and $F_{\mathrm{in},3}/F_{\mathrm{o},3}$ in Figs. 20(a) and 20(b).

In Fig. 20(a), $I_{\mathrm{in}2}$ is the current flowing into the port from the battery when port $F_{\mathrm{in},2}/F_{\mathrm{o},2}$ is assigned as an input port, i.e., $F_{\mathrm{in},2}$. In Period 1, the battery connecting $F_{\mathrm{in},2}$ is supplying power, i.e., power is flowing into the port in this period. Thus, there is no output current of this port. The driving signal of $S_{\mathrm{D}2}$ is $Q_{\mathrm{D}2}$. In Period 2, the port is assigned as an output port, i.e., $F_{\mathrm{o},2}$. Here, power is flowing from the port to the load. The output current of this port is 750 mA, as given in Table IV.

Since port $F_{\mathrm{in},3}/F_{\mathrm{o},3}$ follows the same working principle as port $F_{\mathrm{in},2}/F_{\mathrm{o},2}$, the working waveforms of $F_{\mathrm{in},3}/F_{\mathrm{o},3}$ are similar to those of $F_{\mathrm{in},2}/F_{\mathrm{o},2}$. In Fig. 20(b), $I_{\mathrm{in}3}$ is the current flowing into the port when port $F_{\mathrm{in},3}/F_{\mathrm{o},3}$ is assigned as an input port, i.e., $F_{\mathrm{in},3}$. The driving signal of $S_{\mathrm{D}3}$ is $Q_{\mathrm{D}3}$. When the port is working as an output port (i.e., $F_{\mathrm{o},3}$), the current is flowing into the battery connecting the port. The output current is 400 mA, as designed in Table IV. The bidirectional power flow at the reconfigurable ports can be realized.

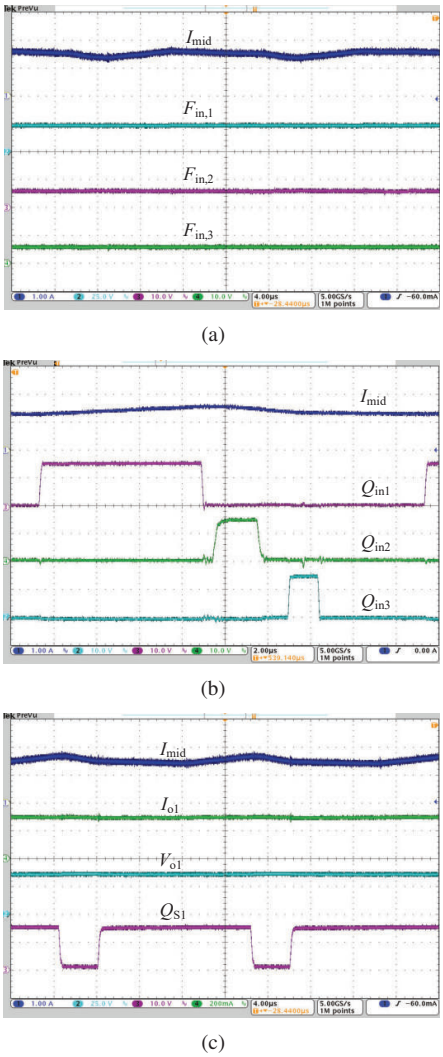

Fig. 19. MISO working waveforms. (a) Input voltages and inductor current of input-side converters; (b) driving signals of $S_{\mathrm{in},1}$, $S_{\mathrm{in},2}$, and $S_{\mathrm{in},3}$ of input-side converters; (c) output voltage and inductor current of the output-side converter.

VII. Discussion on Practical Use

Our focus in this paper is on the topological design and working principles of reconfigurable multiport converters. In practice, due consideration should be given to the factors affecting the performance of the different configurations such as efficiency and grounding arrangements when the circuit is being reconfigured. Here, we provide a brief discussion of the practical aspects of reconfigurable multiport converters, the aim being to facilitate initial design choice. Details of practical circuit design are, however, omitted in this study.

The measured efficiency of the illustrative converter without optimization is shown in Fig. 21. It is obvious that the power dissipated in switches, diodes and the inductor is significant when the output power is in the light to medium range, and satisfactory efficiency is expected for heavy load range. Moreover, the overall efficiency can be optimized using novel power devices and lowering the inductor current. Practical design optimization should warrant a separate in-depth study.

The converter shown in Fig. 8(a) has series-connected input and output ports. Therefore, input sources and output loads should not share a common ground. In this case, PV panels, batteries, and LEDs are suitable terminal devices. Input sources and regenerative loads of the SP connected converter (shown in Fig. 8(b)) should not require grounding arrangement. However, the series connection of the inputs shown in Fig. 8(a) and Fig. 8(b) is a simple way to get a high system voltage without adding another converter for voltage boosting. For the converter with PS connection given in Fig. 8(c), the loads should require no grounding requirement. Moreover, this converter can realize a high voltage step-down ratio due to its series-connected outputs. Furthermore, the converter with PP connection shown in Fig. 8(d) can cater for various types of sources and loads. In practice, however, the switching times of switches at the input side and output side should be duly considered in the control schemes. As the reconfigurable multiport converters are expected to have numerous application opportunities, further study focusing on

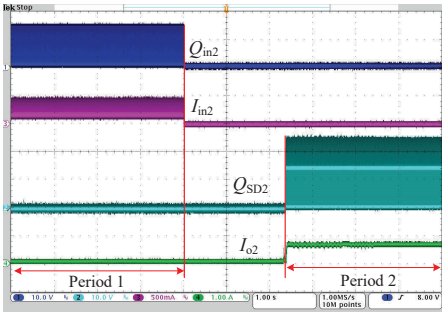

(a)

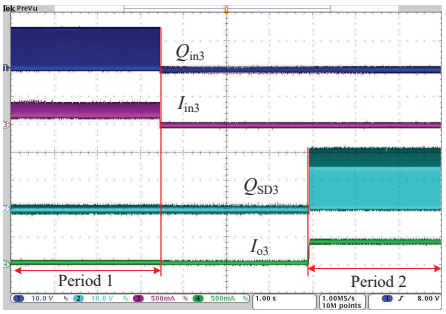

(b)

Fig. 20. Working waveforms of port transition. (a) $F_{\mathrm{in},2}/F_{\mathrm{o},2}$; (b) $F_{\mathrm{in},3}/F_{\mathrm{o},3}$.

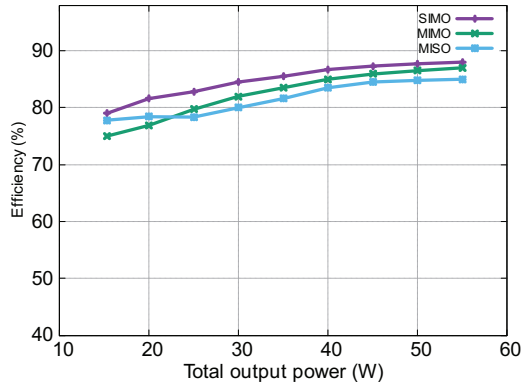

Fig. 21. Measured efficiency of the illustrative configuration.

design optimization should be encouraged.

VIII. Conclusion

In this paper, we propose a systematic method to derive reconfigurable multiport converters with features of reconfigurable ports, no cross regulation and high control design flexibility. Meanwhile, single-inductor structure, high modularity, and high scalability are also maintained. Reconfigurable single-inductor multiport converters provide an economical choice for transforming among single-input multi-output converters, multi-input single-output converters, and multi-input multi-output converters. Using the reconfigurable ports, power can flow bidirectionally and regenerative loads can be integrated flexibly. Unlike conventional design which has cross-regulation issues, the proposed converters have independent output ports while maintaining the single-inductor design. The naturally decoupled output ports enable a simple control scheme to be used, thus avoiding substantial control effort and costly design. Various control schemes can be adopted as long as the simple control principles are followed. Since the proposed converters are constructed from voltage-source-mode dc-dc cells and current-source-mode dc-dc cells, high modularity and an arbitrary number of inputs/outputs are achieved. It should be noted that more multiport configurations can be obtained through different connection styles of voltage-source-mode cells and current-source-mode cells without requiring inductors. Reconfigurable paths can also be established according to the derivation method described in this paper. An illustrative example has been presented to validate the proposed reconfigurable single-inductor multiport converters. A comparison between existing multiport converters with bidirectional power flow function and the derived converters demonstrates the advantages of the derived converters and allows quick selection of configuration for specific applications.

References

[1] A. Payman, S. Pierfederici, and F. Meibody-Tabar, "Energy management in a fuel cell/supercapacitor multisource/multiload electrical hybrid system," *IEEE Trans. Power Electron.*, vol. 24, no. 12, pp. 2681–2691, Dec. 2009.

[2] J. Cao and A. Emadi, "A new battery/ultracapacitor hybrid energy storage system for electric, hybrid, and plug-in hybrid electric vehicles," *IEEE Trans. Power Electron.*, vol. 27, no. 1, pp. 122–132, Jan. 2011.

[3] H. Behjati and A. Davoudi, "Power budgeting between diversified energy sources and loads using a multiple-input multiple-output DC–DC converter," *IEEE Trans. Ind. Appl.*, vol. 49, no. 6, pp. 2761–2772, Jun. 2013.

[4] Y. Tong, Z. Shan, C. N. M. Ho, and J. Jatskevich, "Concept of synthesizing modular power supply for interfacing diverse energy sources and loads," in *Proc. IEEE Workshop Control Model. Power Electron.*, 2015, pp. 1–5.

[5] G. Yu, K. W. R. Chew, Z. C. Sun, H. Tang, and L. Siek, "A 400 nw single-inductor dual-input–tri-output DC–DC buck–boost converter with maximum power point tracking for indoor photovoltaic energy harvesting," *IEEE J. Solid-State Circuits*, vol. 50, no. 11, pp. 2758–2772, Nov. 2015.

[6] S. S. Amin and P. P. Mercier, "MISIMO: A multi-input single-inductor multi-output energy harvesting platform in 28-nm FDSOI for powering net-zero-energy systems," *IEEE J. Solid-State Circuits*, vol. 53, no. 12, pp. 3407–3419, Dec. 2018.

[7] W. Jiang and B. Fahimi, "Multiport power electronic interface – concept, modeling, and design," *IEEE Trans. Power Electron.*, vol. 26, no. 7, pp. 1890–1900, Jul. 2011.

[8] K. P. Yalamanchili, M. Ferdowsi, and K. Corzine, "New double input DC-DC converters for automotive applications," in *Proc. IEEE Veh. Power Propulsion. Conf.*, 2006, pp. 1–6.

[9] H. Behjati and A. Davoudi, "A multiple-input multiple-output DC–DC converter," *IEEE Trans. Ind. Appl.*, vol. 49, no. 3, pp. 1464–1479, Mar. 2013.

[10] Y. Tong, J. Jatskevich, and A. Davoudi, "Topology design of isolated multiport converters for smart dc distribution systems," in *Proc. IEEE Appl. Power Electron. Conf. Expo.*, 2015, pp. 2678–2683.

[11] H. Wu, J. Zhang, and Y. Xing, "A family of multiport buck–boost converters based on DC-link-inductors (DLIs)," *IEEE Trans. Power Electron.*, vol. 30, no. 2, pp. 735–746, Feb. 2014.

[12] Y. Tong, Z. Shan, J. Jatskevich, and A. Davoudi, "A nonisolated multiple-input multiple-output dc-dc converter for dc distribution of future energy efficient homes," in *Proc. 40th Annu. Conf. IEEE Ind. Electron. Soc.*, 2014, pp. 4126–4132.

[13] P. Mohseni, S. H. Hosseini, M. Sabahi, T. Jalilzadeh, and M. Maalandish, "A new high step-up multi-input multi-output DC–DC converter," *IEEE Trans. Ind. Electron.*, vol. 66, no. 7, pp. 5197–5208, Jul. 2018.

[14] G. Chen, Y. Liu, X. Qing, and F. Wang, "Synthesis of integrated multiport DC–DC converters with reduced switches," *IEEE Trans. Ind. Electron.*, vol. 67, no. 6, pp. 4536–4546, Jun. 2019.

TABLE V
COMPARISON WITH EXISTING DESIGNS

References	[29]	[30]	[31]	[32]	[33]	This Work
Number of inductors	1	1	1 coupled inductor	$\geq$1	1 coupled inductor	1
Number of ports	3	3	3	3	3	$m+n$
Scalability of inputs	Low	Low	Low	Low	Low	High
Scalability of outputs	Low	Low	Low	Low	Low	High
Common ground	Yes	No	No	Yes	Yes	Depends on structure
Cross regulation	Yes	Yes	Yes	Yes	Yes	No
Modular level	Low	Low	Low	Low	Low	High
Inductor current	Variable	Variable	Variable	Variable	Variable	Constant

[15] Z. Shan, X. Ding, J. Jatskevich, and C. K. Tse, "Synthesis of multi-input multi-output DC/DC converters without energy buffer stages," *IEEE Trans. Circuits Syst. II, Exp. Briefs*, vol. 68, no. 2, pp. 712–716, Feb. 2021.

[16] C. P. R. Lin and K. Liu, "Family of single-inductor multi-output DC–DC converters," in *Proc. IEEE Int. Conf. Power Electron. Drive Syst.*, 2009, pp. 1216–1221.

[17] D. Kwon and G. A. Rincon-Mora, "Single-inductor-multiple-output switching DC–DC converters," *IEEE Trans. Circuits Syst. II, Exp. Briefs*, vol. 56, no. 8, pp. 614–618, Aug. 2009.

[18] K. Gummi and M. Ferdowsi, "Double-input DC–DC power electronic converters for electric-drive vehicles—topology exploration and synthesis using a single-pole triple-throw switch," *IEEE Trans. Ind. Electron.*, vol. 57, no. 2, pp. 617–623, Feb. 2010.

[19] J. P. Agrawal, "Determination of cross regulation in multioutput resonant converters," *IEEE Trans. Aerosp. Electron. Syst.*, vol. 36, no. 3, pp. 760–772, Mar. 2000.

[20] Z. Shen, X. Chang, W. Wang, X. Tan, N. Yan, and H. Min, "Predictive digital current control of single-inductor multiple-output converters in CCM with low cross regulation," *IEEE Trans. Power Electron.*, vol. 27, no. 4, pp. 1917–1925, Apr. 2012.

[21] P. Patra, J. Ghosh, and A. Patra, "Control scheme for reduced cross-regulation in single-inductor multiple-output DC–DC converters," *IEEE Trans. Ind. Electron.*, vol. 60, no. 11, pp. 5095–5104, Nov. 2012.

[22] B. Wang, V. R. K. Kanamarlapudi, L. Xian, X. Peng, K. T. Tan, and P. L. So, "Model predictive voltage control for single-inductor multiple-output DC–DC converter with reduced cross regulation," *IEEE Trans. Ind. Electron.*, vol. 63, no. 7, pp. 4187–4197, Jul. 2016.

[23] B. Wang, L. Xian, V. R. K. Kanamarlapudi, K. J. Tseng, A. Ukil, and H. B. Gooi, "A digital method of power-sharing and cross-regulation suppression for single-inductor multiple-input multiple-output DC–DC converter," *IEEE Trans. Ind. Electron.*, vol. 64, no. 4, pp. 2836–2847, Apr. 2016.

[24] B. Wang, X. Zhang, J. Ye, and H. B. Gooi, "Deadbeat control for a single-inductor multiple-input multiple-output DC–DC converter," *IEEE Trans. Power Electron.*, vol. 34, no. 2, pp. 1914–1924, Feb. 2018.

[25] E. Bonizzoni, F. Borghetti, P. Malcovati, F. Maloberti, and B. Niessen, "A 200mA 93% peak efficiency single-inductor dual-output DC-DC buck converter," in *Proc. IEEE Solid-State Circuits Conf*, 2007, pp. 526–619.

[26] X. L. Li, Z. Dong, and C. K. Tse, "Series-connected current-source-mode multiple-output converters with high step-down ratio and simple control," *IEEE Trans. Power Electron.*, vol. 34, no. 10, pp. 10 082–10 093, Oct. 2019.

[27] X. L. Li, Z. Dong, C. K. Tse, and D. D.-C. Lu, "Single-inductor multi-input multi-output DC–DC converter with high flexibility and simple control," *IEEE Trans. Power Electron.*, vol. 35, no. 12, pp. 13 104–13 114, Dec. 2020.

[28] Z. Dong, X. L. Li, C. K. Tse, and Z. Zhang, "Derivation of single-input dual-output converters with simple control and no cross regulation," *IEEE Trans. Power Electron.*, vol. 35, no. 11, pp. 11 930–11 941, Nov. 2020.

[29] T. Cheng, D. D.-C. Lu, and L. Qin, "Non-isolated single-inductor DC/DC converter with fully reconfigurable structure for renewable energy applications," *IEEE Trans. Circuits Syst. II, Exp. Briefs*, vol. 65, no. 3, pp. 351–355, Mar. 2017.

[30] P. Zhang, Y. Chen, and Y. Kang, "Nonisolated wide operation range three-port converters with variable structures," *IEEE J. Emerg. Sel. Topics Power Electron.*, vol. 5, no. 2, pp. 854–869, May 2017.

[31] M. R. Al-Soeidat, H. Aljarajreh, H. A. Khawaldeh, D. D.-C. Lu, and J. Zhu, "A reconfigurable three-port DC–DC converter for integrated PV-battery system," *IEEE J. Emerg. Sel. Topics Power Electron.*, vol. 8, no. 4, pp. 3423–3433, Apr. 2019.

[32] H. Wu, K. Sun, S. Ding, and Y. Xing, "Topology derivation of nonisolated three-port DC–DC converters from DIC and DOC," *IEEE Trans. Power Electron.*, vol. 28, no. 7, pp. 3297–3307, Jul. 2012.

[33] R. Faraji, L. Ding, M. Esteki, N. Mazloum, and S. A. Khajehoddin, "Soft-switched single inductor single stage multiport bidirectional power converter for hybrid energy systems," *IEEE Trans. Power Electron.*, vol. 36, no. 10, pp. 11 298–11 315, Oct. 2021.

[34] Z. Dong, C. K. Tse, and S. Y. R. Hui, "Circuit theoretic considerations of led driving: voltage-source versus current-source driving," *IEEE Trans. Power Electron.*, vol. 34, no. 5, pp. 4689–4702, May 2019.

[35] C. K. Tse, *Linear Circuit Analysis*. London: Addison-Wesley, 1998.

[36] X. L. Li, Z. Dong, and C. K. Tse, "Complete family of two-stage single-input multioutput configurations of interconnected power converters," *IEEE Trans. Power Electron.*, vol. 35, no. 4, pp. 3713–3728, Apr. 2020.

Xiaolu Lucia Li (M'19) received the B.Eng. and M.Phil. degrees in electrical engineering from Harbin Institute of Technology, Harbin, China, in 2014 and 2016, respectively, and the Ph.D. degree in power electronics from Hong Kong Polytechnic University, Hong Kong, in 2019. After graduation, she worked briefly as a Research Assistant in Pong Yuen Holdings Limited, Hong Kong. She is presently a Postdoctoral Fellow with the Department of Electrical Engineering at City University of Hong Kong. Her research interests include multiport converters and wireless power transfer.

Chi K. Tse (M'90–SM'97–F'06) received the BEng (Hons) degree with first class honors in electrical engineering and the PhD degree from the University of Melbourne, Australia, in 1987 and 1991, respectively.

He is presently Associate Vice President (Research) and Chair Professor of Electrical Engineering at City University of Hong Kong, Hong Kong. Prior to joining City University of Hong Kong in October 2019, he was with Hong Kong Polytechnic University, with which he served as Head of the Department of Electronic and Information Engineering from 2005 to 2012. His research interests include power electronics, nonlinear systems and complex network applications. He pioneered the research in nonlinear dynamics of power electronics in the early 1990s and has extended the research direction to grid-connected power converters.

Dr. Tse was recipient of a number of research and invention prizes including a few Best Paper Prizes from IEEE and other journals, as well as a Grand Prize in Silicon Valley International Invention Festival (2019). In 2005, 2010 and 2018, he was selected and appointed as IEEE Distinguished Lecturer. In 2006 he chaired the IEEE CAS Technical Committee on Nonlinear Circuits and Systems. He serves and has served as Editor-in-Chief of IEEE Transactions on Circuits and Systems II (2016-2019), IEEE Circuits and Systems Magazine (2013-2016), IEICE Nonlinear Theory and Applications (since 2013); as Editor of IJCTA (2014-2020); as associate editor of a few other IEEE journals; and on the Editorial Board of IEEE Proceedings. He has served on a number of IEEE committees including the IEEE Fellows Committee and the IEEE Awards Committee, and chaired the Steering Committee for IEEE Transactions on Network Science and Engineering. He has been appointed to honorary professorship and distinguished fellowship by a few Australian, Canadian and Chinese universities, including the Chang Jiang Scholar Chair Professor with Huazhong University of Science and Technology, Honorary Professor of Melbourne University, and Distinguished Professor-at-Large with the University of Western Australia. He also served as panel member of Hong Kong Research Grants Council, and member of several professional and government committees.

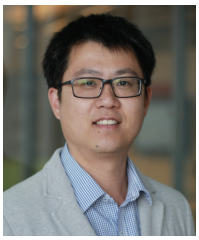

Dylan Dah-Chuan Lu (M'04–SM'09) received his Ph.D. degree in electronic and information engineering in 2004, from the Hong Kong Polytechnic University, Hong Kong. In 2003, he joined Power^e Lab Ltd. as a Senior Design Engineer where he was responsible for industrial switching power supply projects. He was a full-time faculty member with The University of Sydney, Australia, from 2006 to 2016, where he now holds an Honorary position. He joined University of Technology Sydney, Australia, in July 2016. He is currently a Professor and Head of Discipline of Electrical Power and Energy Systems at the School of Electrical and Data Engineering. His current research interest and publications focus on efficient, cost-effective and reliable power conversion for renewable energy sources, energy storage systems, and microgrids. He is presently serving as Chair of the Joint Chapter IAS/IES/PELS (IEEE New South Wales Section) and an Associate Editor of the *IEEE Transactions on Industrial Electronics* and the *IEEE Journal of Emerging and Selected Topics in Power Electronics*.